JOURNAL OF Materials CHEMISTRY

Magnetic and electronic properties of lead-doped lanthanum manganate

Anthony V. Powell,*[a] Christian Herwig,[a] Douglas C. Colgan[a] and A. Gavin Whittaker[b]

[a]*Department of Chemistry, Heriot-Watt University, Riccarton, Edinburgh, UK EH14 4AS*
[b]*Department of Chemistry, University of Edinburgh, King's Buildings, West Mains Road, Edinburgh, UK EH9 3JJ*

Materials of nominal composition $La_{1-x}Pb_xMnO_3$ ($0.0 \leqslant x \leqslant 0.4$) prepared by prolonged annealing at 950 °C, have been characterised by a combination of powder X-ray diffraction, energy dispersive X-ray microanalysis, thermogravimetry, atomic absorption spectroscopy and oxidising-power analysis. All phases adopt a rhombohedral variant of the perovskite structure and show significant deviations from nominal stoichiometries. All doped materials exhibit ferromagnetic ordering at a temperature, T_C, close to ambient and undergo a metal–insulator transition at a temperature, T_{MI}, close to T_C. Both T_C and T_{MI} show greater compositional variation than previously reported.

The exceptional magnetotransport properties exhibited by perovskite-like phases of general formula $Ln_{1-x}A_xMnO_3$ (A = Ca, Ba, Sr, Pb) has led to a recent explosion of interest in mixed manganese oxides.[1–3] In certain compositional regions, corresponding to the range of oxidation states between $Mn^{III}:t_{2g}^3e_g^1$ and $Mn^{IV}:t_{2g}^3$, ferromagnetic ordering occurs below the Curie temperature T_C. There is a sharp drop in resistance at temperatures close to T_C; electronic properties above and below T_C are characteristic of insulating and metallic behaviour, respectively. The metal–insulator (MI) transition occurs at a temperature, T_{MI}, in the same temperature window as T_C. The measured resistance is strongly dependent on external magnetic fields and the materials exhibit giant magnetoresistance (GMR), characterised by negative values of the ratio $\Delta\rho/\rho_0$ [$\Delta\rho$ is the difference between resistivity measured in a field (ρ_H) and that measured in zero field (ρ_0)] which frequently approach -1.[4] GMR is most marked at temperatures in the region of T_C/T_{MI}, suggesting that it is closely linked to MI behaviour and ferromagnetism. Theoretical understanding of the properties of these materials is not well developed, although it appears that the mechanism is not the order–disorder type operative in metallic multilayers, and alternative models have been proposed.[5–7] Attainment of a consistent theoretical picture is complicated by discrepancies in properties determined for materials prepared under different conditions. Direct correspondence between materials of the same nominal composition prepared in thin-film, single crystal or polycrystalline forms is not consistently observed. Moreover, annealing further modifies these properties.

The temperatures T_C, T_{MI} and the magnetoresistance are influenced by a subtle interplay between the number of charge carriers, determined primarily by the degree of doping, and the microstructural properties; in particular the Mn—O distances and Mn—O—Mn angles, which are themselves composition dependent. These materials provide opportunities to tailor properties to specific applications by chemical control and initial studies indicate that magnetic and electronic properties are extremely sensitive to minor compositional changes.[8,9] Applications are readily apparent in the information storage industry where magnetoresistive read-heads offer potentially greater storage densities than possible with inductive devices.[10] However, properties such as a large $\Delta\rho/\rho_0$ and high sensitivity to magnetic fields, need to be realised at or close to ambient temperatures. Epitaxial films of mixed manganese oxides including La–Ca–Mn–O ($\Delta\rho/\rho_0 = -0.52$ at 22 K, 10 kG)[11] and La–Ba–Mn–O ($\Delta\rho/\rho_0 = -0.32$ at 300 K, 65 kG)[12] exhibit promising characteristics. Similar properties have been observed in polycrystalline materials,[13] demonstrating that epitaxial growth is not an essential prerequisite.

We have recently commenced an investigation of lead-doped materials of general formula $La_{1-x}Pb_xMnO_3$ for which critical temperatures close to 300 K have been reported[14] within the composition range $0.1 \leqslant x \leqslant 0.5$. Hence, these materials offer the possibility of realising a technologically useful magnetoresistive effect at temperatures close to ambient. Indeed, a $\Delta\rho/\rho_0$ of -0.4 at 300 K, 6 T has been observed[15] in thin films of $La_{0.6}Pb_{0.4}MnO_3$. In this work, magnetic and electronic data are presented for carefully characterised samples which have undergone prolonged annealing. These data exhibit greater compositional variations than previously reported.

Experimental

All samples were prepared by standard high-temperature solid-state reactions. Appropriate amounts of lanthanum oxide, lead and manganese powders (Johnson Matthey spectroscopic grade) were ground and pelletised prior to firing in an alumina crucible at 950 °C in air. Reaction progress was monitored by recording powder X-ray diffraction patterns on a Philips PA2000 diffractometer, at periodic intervals, prior to re-grinding, pelletising and returning to the furnace. Products from the initial firings appeared to be sensitive to atmospheric moisture, resulting in visible degradation of the sample and loss of mechanical integrity of the sintered pellet. For this reason, all reaction products were handled under an atmosphere of dry nitrogen and an X-ray sample holder, which enabled the sample to be kept in a nitrogen atmosphere during data collection, was used. Although the product phase formed rapidly, powder X-ray diffraction patterns indicated the presence of trace amounts of lanthanum oxide even after several days of heating. Repeated firings over a period of 20–36 days were necessary to remove all of the binary oxide contaminant. On completion of the reaction, powder X-ray diffraction data were collected in step-scan mode over the angular range $10 \leqslant 2\theta \leqslant 100°$ using a step-size of $2\theta = 0.02°$ and a counting time of 5 s step^{-1}.

Energy dispersive microanalysis was performed with a JEOL 200FX electron microscope fitted with a Tracor Northern analysis system. Oxygen contents were determined thermogravimetrically by reduction in a flowing H_2–Ar mixture (8% H_2) using a Stanton Redcroft STA-780 thermal analyser.

Table 1 Results of thermogravimetry, redox titration and energy dispersive X-ray microanalysis for the mixed manganese oxides

nominal composition	manganese content(%)	weight loss on reduction(%)	oxidising power/e^- (mg of sample)$^{-1}$	La : Mn[a]	experimentally determined composition[b]	oxidation state of Mn v(Mn)	I(La−Lα)/I(Pb−Mα) in X-ray microanalysis
$LaMnO_3$	21.7(1)	4.05(6)	4.92(4)	standard	$La_{0.99}Mn_{0.93}O_3$	3.26	—
$La_{0.9}Pb_{0.1}MnO_3$	21.7(1)	3.99(5)	5.1(3)	0.97(5)	$La_{0.94}Pb_{0.07}Mn_{0.97}O_3$	3.13	7.6(7)
$La_{0.8}Pb_{0.2}MnO_3$	21.5(1)	5.11(5)	4.75(9)	0.88(6)	$La_{0.84}Pb_{0.13}Mn_{0.96}O_3$	3.35	3.3(4)
$La_{0.7}Pb_{0.3}MnO_3$	20.79(4)	5.67(9)	4.9(2)	0.89(3)	$La_{0.82}Pb_{0.15}Mn_{0.92}O_3$	3.52	2.5(2)
$La_{0.6}Pb_{0.4}MnO_3$	21.83(3)	6.36(9)	5.17(1)	0.79(5)	$La_{0.74}Pb_{0.16}Mn_{0.94}O_3$	3.68	1.9(2)

[a]By X-ray microanalysis. [b]Estimated uncertainties are in the second decimal place.

Products of reduction were identified by powder X-ray diffraction. Manganese contents were determined spectrophotometrically. The oxidising power of the samples was determined by a redox titration, involving dissolution of known weights of sample in excess acidified ammonium iron(II) sulfate solution followed by back titration with potassium permanganate.

Magnetic susceptibility measurements on powdered samples were made using a Quantum Design MPMS2 SQUID susceptometer. Samples were transferred to gelatin capsules under an atmosphere of dry nitrogen and were loaded at room temperature in zero magnetic field. Measurements were taken in the temperature range 6–350 K, both after cooling the sample in zero-field (zfc) and after cooling in the measuring field (fc) of 0.1 kG. Samples were then re-cooled to 10 K in the measuring field and the magnetisation measured as a function of applied field in the range 0.1–10 kG.

Electrical resistance measurements were made using the four-probe DC technique. Ingots (*ca.* $6\times3\times1$ mm) were cut from sintered pellets, four 50 μm silver wires were attached using colloidal silver paint and connections made to a HP34401A multimeter. Data were collected between 100 and 300 K ($0.0\leqslant x\leqslant0.2$) or 400 K ($x=0.3$, 0.4) by placing the sample in an Oxford Instruments CF1200 cryostat connected to an ITC502 temperature controller.

Results

Analytical data are presented in Table 1. Sample compositions were obtained as follows. A combination of thermogravimetry (TG) and atomic absorption spectroscopy (AAS) allowed the composition of the undoped material to be determined as $La_{0.99}Mn_{0.93}O_3$. An identical result was obtained using a combination of the redox titration and atomic absorption spectroscopy. This sample of lanthanum manganate of analytically determined composition was subsequently used as a La : Mn intensity standard for X-ray microanalysis. This permitted the La : Mn ratio to be determined for the doped materials. Using this ratio, in conjunction with the results of TG and AAS, the experimental compositions of Table 1 were obtained. Making use of data from the redox titrations in place of those from the TG led to slightly different compositions for the more heavily doped materials. This appeared to be related to the precipitation of a lead salt during the redox analysis of these samples which interfered with the end-point of the titrations. For this reason, we believe that the TG-derived compositions are more reliable and it is these which are given in Table 1.

All of the most intense peaks in the powder X-ray diffraction pattern of $La_{0.99}Mn_{0.93}O_3$ could be indexed on the basis of a rhombohedral unit cell with $a\approx5.4$ Å, $\alpha\approx60^\circ$. However, this left several weak features, including peaks at 2θ *ca.* 25.1, 34.2, 41.4 and 47.7°, unindexed. This unit cell may be considered as the primitive unit cell of a larger face-centred rhombohedral unit cell which is more obviously related to a doubled ($2a\times2a\times2a$) cubic perovskite unit cell. All peaks in the diffraction pattern could be indexed on the basis of this enlarged unit cell, with the face-centring condition removed. The weak additional features were absent from the profiles of the doped phases, data for which could be indexed on the basis of the smaller rhombohedral unit cell. However, at higher levels of doping (nominal $x\geqslant0.3$), a weak reflection (relative intensity $\leqslant0.01$) is observed at 2θ *ca.* 36°. This may be assigned as the (211) reflection of Mn_3O_4 ($d_{calc}=2.487$ Å), trace amounts of which introduce slightly larger uncertainties into the analytically determined compositions of these two phases.

As a further check on phase purity of the materials, Rietveld refinement of powder diffraction data was carried out.† Initial structural models, including approximate atomic coordinates for the doubled unit cell of $La_{0.99}Mn_{0.93}O_3$, were derived from the parameters of Tofield and Scott.[16] Compositions were constrained to their analytically determined values. Although refinements were of sufficient quality (R_{wp} *ca.* 6–10%) to establish phase purity unambiguously, problems were encountered in refining the positional and thermal parameters of oxygen. This may be traced to the lack of sensitivity of X-rays to the oxide sub-lattice in the presence of strong scatterers such as lead. At higher levels of doping ($x\geqslant0.3$), the oxygen (x, $\bar{x}+½$, ¼) positional parameter, x, became unstable and oscillated about 0.75. This is linked to the gradual removal of the rhombohedral distortion at higher lead contents leading to values of x which approach 0.75 closely. For these reasons, it would be inappropriate to report full details of the refinements here and we restrict ourselves to the unit-cell parameters which are given in Table 2. Detailed structural studies using powder neutron diffraction are currently in progress and details will be reported in due course. Magnetic susceptibility data for the undoped material, $La_{0.99}Mn_{0.93}O_3$, are shown in Fig. 1. At higher temperatures, zfc and fc susceptibilities overlie each other completely. Magnetic susceptibility increases in the temperature range $150\leqslant T\leqslant175$ K. At lower temperatures, zfc and fc curves diverge and the zfc curve shows a maximum susceptibility at $T\approx110$ K. Fitting the data above $T=245$ K to a Curie–Weiss law resulted in the parameters $\theta=192(2)$ K and $C=3.97(2)$ emu K^{-1}.

Magnetic susceptibility data for the doped materials are shown in Fig. 2–5. In all cases, zfc and fc data overlie each other at higher temperatures. A sharp increase in measured susceptibility, indicative of the onset of ferromagnetic ordering, occurs for the mixed phases. The Curie temperature, T_C,

Table 2 Unit-cell parameters for the mixed manganese oxides (space group $R\bar{3}c$)

composition	a/Å	α/°	V/Å^3
$La_{0.99}Mn_{0.93}O_3$	7.787(2)	90.20(1)	472.2(4)[a]
$La_{0.94}Pb_{0.07}Mn_{0.97}O_3$	5.4942(2)	60.600(2)	118.86(1)[b]
$La_{0.84}Pb_{0.13}Mn_{0.96}O_3$	5.4956(3)	60.595(1)	118.94(1)[b]
$La_{0.82}Pb_{0.15}Mn_{0.92}O_3$	5.4972(2)	60.574(1)	118.99(1)[b]
$La_{0.74}Pb_{0.16}Mn_{0.94}O_3$	5.4982(2)	60.487(1)	118.82(1)[b]

[a]$Z=8$. [b]$Z=2$.

† Available as supplementary material (**SUP 57306**; 3 pp.) deposited with the British Library. Details are available from the editorial office.

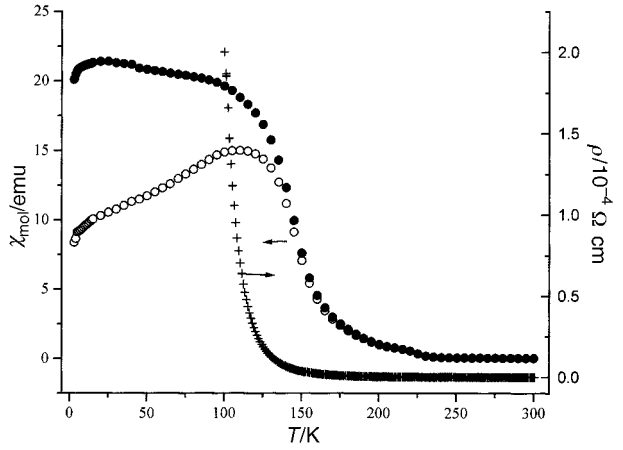

Fig. 1 Temperature variation of the zero-field cooled (zfc; ○) and field-cooled (fc; ●) molar magnetic susceptibilities and the electrical resistivity (ρ) of $La_{0.99}Mn_{0.93}O_3$

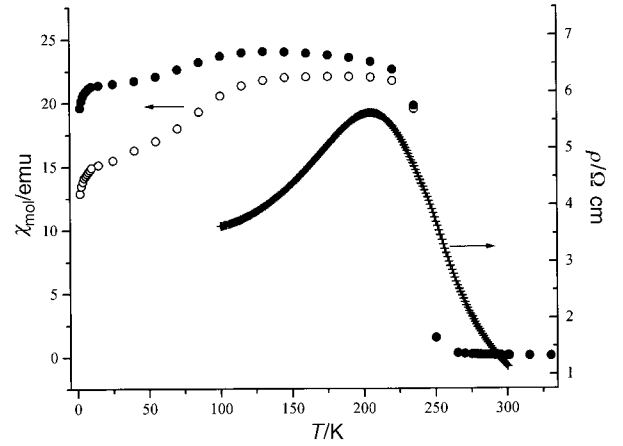

Fig. 2 Temperature variation of the zero-field cooled (zfc; ○) and field-cooled (fc; ●) molar magnetic susceptibilities and the electrical resistivity (ρ) of $La_{0.94}Pb_{0.07}Mn_{0.97}O_3$

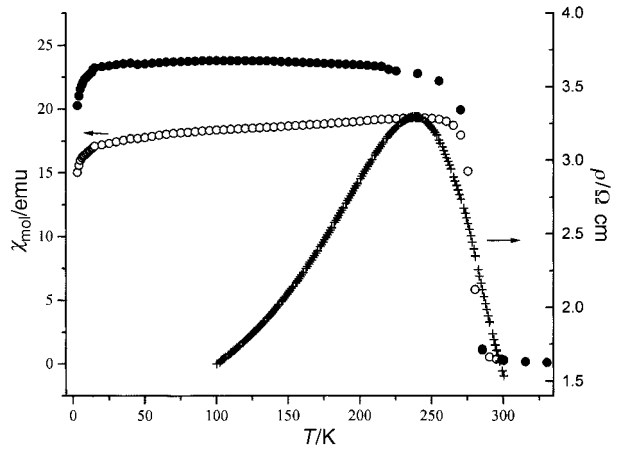

Fig. 3 Temperature variation of the zero-field cooled (zfc; ○) and field-cooled (fc; ●) molar magnetic susceptibilities and the electrical resistivity (ρ) of $La_{0.84}Pb_{0.13}Mn_{0.96}O_3$

determined from the maximum value of $\partial\chi/\partial T$, increases with increasing lead content (Table 3). Measurements carried out in a measuring field of 1 kG indicated that T_C is not significantly affected by the magnitude of the measuring field. The zfc and fc curves diverge below T_C with the latter lying above that obtained on zero-field-cooling as a result of increased alignment of ferromagnetic domains on cooling in the presence of a field. A sharp discontinuity is evident at *ca.* 50 K in the data

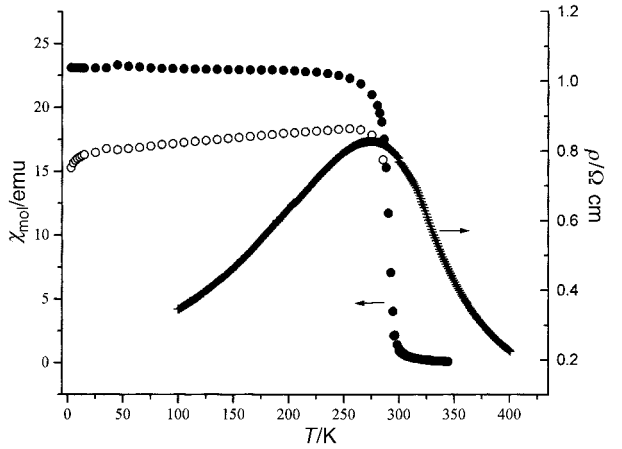

Fig. 4 Temperature variation of the zero-field cooled (zfc; ○) and field-cooled (fc; ●) molar magnetic susceptibilities and the electrical resistivity (ρ) of $La_{0.82}Pb_{0.15}Mn_{0.92}O_3$

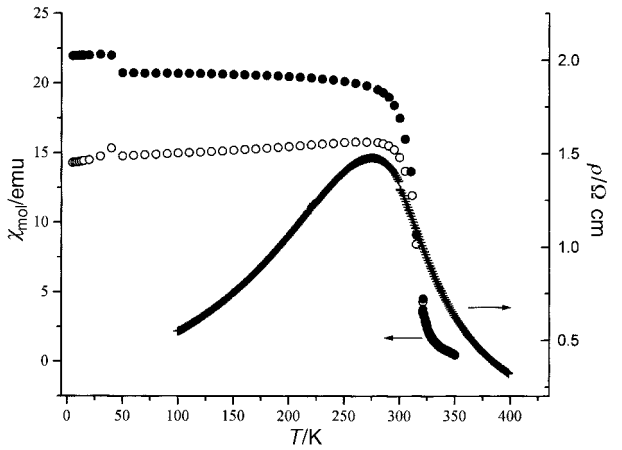

Fig. 5 Temperature variation of the zero-field cooled (zfc; ○) and field-cooled (fc; ●) molar magnetic susceptibilities and the electrical resistivity (ρ) of $La_{0.74}Pb_{0.16}Mn_{0.94}O_3$

for $La_{0.74}Pb_{0.16}Mn_{0.94}O_3$. This is likely to be a consequence of magnetic ordering of the trace amount of Mn_3O_4 ($T_c = 43$ K) present. However, this ordering temperature is sufficiently far removed from T_C to have little effect on the magnetic ordering temperature of the bulk phase. Values of the low-temperature saturated moments (μ_{sat}) were obtained from the field dependence of the magnetisation (Fig. 6) by taking the intercept on the moment-axis of linear fits to the high-field region of moment *vs.* $1/H$ plots. These values are given in Table 3.

For ready comparison of magnetic and electronic properties, the temperature variation of resistivity (ρ) is given on the same plots as the magnetic susceptibilities in Fig. 2–5. The undoped material is semiconducting with $\rho_{100\ K} = 2 \times 10^4$ Ω cm. For the doped materials, resistivity initially increases with decreasing temperature. However, maxima in $\rho(T)$ are observed at lower temperatures. The maximum value of the resistivity for the doped materials is up to four orders of magnitude lower than the maximum value of ρ for $La_{0.99}Mn_{0.93}O_3$. The temperature at which ρ_{max} occurs may be identified as the temperature of the metal–insulator (MI) transition in these materials, T_{MI} (Table 3).

Discussion

The sample of lanthanum manganate prepared during the course of this work contains an appreciable amount of Mn^{4+} (*ca.* 26%), in accord with previous observations of oxidative non-stoichiometry in $LaMnO_3$.[17] It has been shown[18] that

Table 3 Summary of magnetic and electronic data for the mixed manganese oxides

composition	T_C/K	T_{MI}/K	μ_{sat}/μ_B per Mn ion (obs.)	μ_{sat}/μ_B per Mn ion (calc.)
$La_{0.99}Mn_{0.93}O_3$	150(3)	—	3.93(1)	3.74
$La_{0.94}Pb_{0.07}Mn_{0.97}O_3$	244(6)	205(1)	4.05(2)	3.87
$La_{0.84}Pb_{0.13}Mn_{0.96}O_3$	278(3)	240(1)	3.65(2)	3.65
$La_{0.82}Pb_{0.15}Mn_{0.92}O_3$	290(3)	274(1)	3.54(1)	3.48
$La_{0.74}Pb_{0.16}Mn_{0.94}O_3$	318(3)	274(1)	3.11(1)	3.32

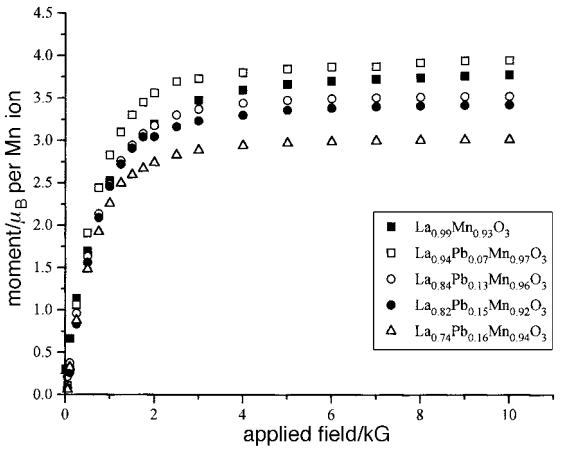

Fig. 6 Variation in the magnetic moment of the prepared materials as a function of applied magnetic field

preparation of the stoichiometric orthorhombic phase requires reducing conditions, whereas firing in oxygen or air results in a rhombohedral phase. Wollan and Koehler[19] have reported that $LaMnO_{3+\delta}$ remains orthorhombic for Mn^{4+}-contents of up to approximately 25%. Crystallographic studies by Wold and Arnott[20] place the boundary between room-temperature rhombohedral and orthorhombic structures at 21% Mn^{4+}. Although the precise position of the phase boundary is likely to be sensitive to the La : Mn ratio, 26% Mn^{4+} appears to place the phase in the rhombohedral region of the phase diagram. This is in agreement with the results of Töpfer and Goodenough[21] who have recently presented structural data for lanthanum manganate prepared over a range of La : Mn ratios and oxygen contents.

Powder neutron diffraction data[16] for the rhombohedral phase indicated that there are vacancies on the La and Mn sub-lattices and the compound was formulated with a greater number of the former. A recent study[22] of the relationship between unit-cell volume and the percentage of Mn^{4+} at different La : Mn ratios concluded that the La : Mn ratio in the earlier work had been incorrectly determined and, for a sample with La : Mn = 1.00, powder neutron diffraction indicated an equal number of La and Mn vacancies. The sample prepared here has La : Mn > 1.0 and it is therefore unsurprising that there should be a greater number of Mn than La vacancies. Examination of the plots presented by Van Roosmalen *et al.*[22] indicates that a unit-cell volume of 472 Å^3 ($Z = 8$) for a sample containing 26% Mn^{4+} is consistent with a La : Mn ratio > 1.0, although these plots would suggest a slightly lower ratio than the 1.06 observed.

Orthorhombic lanthanum manganate is antiferromagnetic with a T_N which depends on the Mn^{4+} content.[23] Conversely, the rhombohedral phase has a ferromagnetic ground state and T_C is also composition dependent.[24] Although some discrepancies between T_C derived from neutron and susceptibility data are apparent in the literature,[18] the value determined here is consistent with previously reported values for the rhombohedral phase determined from susceptibility data.[18] Orthorhombic $LaMnO_3$ with a low percentage of Mn^{4+} possesses an effective magnetic moment (μ_{eff}) of 4.8 μ_B in good agreement with the spin-only value.[23] An increase in the mean manganese oxidation state, hereafter denoted v(Mn), decreases μ_{eff} and a value of 4.7 μ_B is calculated for $La_{0.99}Mn_{0.93}O_3$. This is considerably lower than the value of 5.8(1) μ_B determined from the Curie–Weiss fit. A similar enhancement of the spin-only moment has recently been observed[25] in lanthanum manganates, containing manganese in a range of oxidation states, and indicates that in this temperature region, additional short-range magnetic interactions are operating. At considerably higher temperatures ($\leqslant 1000$ K), these interactions are absent and μ_{eff} approaches the spin-only value closely.[26] The present analysis is complicated by the non-linearity of the reciprocal susceptibility plot above T_C. In particular, a second linear region, of steeper gradient, is observed in the temperature range $224 \leqslant T \leqslant 245$ K. The increase in gradient, and hence decrease in C and μ_{eff}, may be associated with the occurrence of a rhombohedral to orthorhombic phase transition at 245 K. Although powder neutron diffraction studies would be required to confirm a phase transition, this transition temperature would be in good agreement with the low-temperature structural studies of Wold and Arnott[20] and the qualitative phase diagram recently presented by Töpfer and Goodenough[25] who observed a similar change in slope in reciprocal susceptibility plots.

Analytically determined compositions of the doped materials show significant deviations from nominal compositions. In particular, lead contents are considerably lower; the loss of lead becoming more marked as the nominal value of x increases. This may be attributed to the volatility, even at the relatively low reaction temperatures utilised here, of the lead oxide produced during the early stages of synthesis. This was confirmed by subsequent firing of samples at 950 °C in a horizontal tube furnace during which single crystals were found to form in the cooler regions of the tube. These were identified as PbO by powder X-ray diffraction. Over the long reaction times used for the preparation of the phases described here, loss of PbO results in significant changes to the La : Pb ratio. The La-Lα/Pb-Mα intensity ratio observed in the X-ray microanalysis (Table 1) provides qualitative support for the lead contents determined analytically. However, the absence of a suitable intensity standard precludes quantitative analysis of the La : Pb ratio by this method. While loss of lead would be expected to result in a smaller variation in v(Mn), and hence in the number of charge carriers, it can be seen that this effect is offset by the presence of significant numbers of vacancies on the manganese sub-lattice. Consequently, after an initial decrease between the undoped material and the sample of nominal composition $x = 0.1$, v(Mn) increases markedly with increasing x.

Goodenough[27] has discussed the composition dependence of the structures of $LaMnO_3$ doped with divalent cations. The orthorhombic structure of stoichiometric $LaMnO_3$ results from bond-ordering of vacant cation orbitals associated with Mn^{3+}. This involves the occupied members of the e_g set of orbitals on adjacent Mn^{3+} ions in the *ab* plane being oriented perpendicular to each other within the plane, resulting in alternate long and short in-plane Mn—O bonds. Introduction of Mn^{4+} on doping destroys this bond-ordering, resulting in smaller

distortions from cubic symmetry. All doped materials reported here, contain significant amounts of Mn^{4+} and adopt a rhombohedrally distorted perovskite structure. The rhombohedral distortion is progressively removed with increasing v(Mn). This trend appears to be continued in the material of nominal composition $La_{0.5}Pb_{0.5}MnO_3$ which has been reported to be cubic.[28]

The manner in which T_C and T_{MI} closely parallel each other indicates that magnetic ordering and the properties of the conduction electrons are closely linked. Oxidation of a greater percentage of $Mn^{3+}:d^4$ to $Mn^{4+}:d^3$ would be expected to lead to a decrease in the saturated moment of the ordered state which is indeed the case. However, saturated moments measured at 10 K are in good agreement with values calculated assuming spin-only behaviour. This suggests that a conventional band picture is an inadequate description of the conduction electrons in the low-temperature metallic state. The double exchange mechanism proposed by Zener[29] provides a rationale for the observed behaviour. This involves hopping of an e_g electron between two t_{2g}^3 cores *via* an intermediate oxide anion such that the states $Mn^{3+}-O-Mn^{4+}$ and $Mn^{4+}-O-Mn^{3+}$ are degenerate. Strong intra-ionic exchange coupling between the transferred electron and the t_{2g}^3 electrons requires the t_{2g}^3 spins to be parallel before electron transfer can occur. In the paramagnetic region, electron hopping occurs in a medium of fluctuating spins and semiconducting behaviour results. The parallel alignment of electron spins in the ferromagnetically ordered state minimises the scattering of charge carriers. Hence the onset of ferromagnetism is accompanied by a decrease in resistivity which continues as the magnetisation increases on further reducing the temperature. It has been pointed out that if Mn^{3+} and Mn^{4+} ions form part of an ordered lattice, in which they occupy crystallographically distinct sites, the degeneracy of the $Mn^{3+}-O-Mn^{4+}$ and $Mn^{4+}-O-Mn^{3+}$ states is removed and double exchange is inhibited.[27] Although ferromagnetism may still be observed, its origin lies in other exchange mechanisms and it is not accompanied by a decrease in resistivity. Charge ordering could account for the semiconducting behaviour of $La_{0.99}Mn_{0.93}O_3$ through the Curie temperature and would be consistent with the enlarged unit cell.

The temperatures T_C and T_{MI} for the doped materials support the general observation that the MI transition occurs below the magnetic ordering temperature. The difference $T_C - T_{MI}$ is within the range commonly observed, although differences as great as *ca.* 200 K have been reported.[30] Both structural and electronic factors affect T_C and hence T_{MI}. At moderate levels of doping, T_C increases with increasing Mn^{4+} content. However, a change in the dopant concentration is inevitably accompanied by structural changes. In particular, substitution alters the average radius of the cation at the twelve-coordinate (A) site. Adjustment of the oxide sub-lattice in order to optimise the coordination by oxygen of the ion at the A site causes tilts and rotations of the MnO_6 octahedra. This results in changes to the microstructure, in particular the Mn—O—Mn angles (ϕ), to which magnetic and electronic properties are especially sensitive, owing to the dependence on $\cos^2\phi$ of the matrix element for electron hopping between sites.

There is a clear correlation between T_C/T_{MI} and v(Mn) as shown in Fig. 7. Both ordering temperatures increase with increasing v(Mn) as anticipated, although T_{MI} appears to reach a saturation value. There are relatively few reports of the composition dependence of T_C/T_{MI} for the lead-doped materials. Well characterised single crystals[14] of $La_{1-x}Pb_xMnO_3$, for which $0.25 \leqslant x \leqslant 0.45$, possess Curie temperatures in the range 320–350 K with T_{MI} spanning the range 315–350 K. Thin films of $La_{0.6}Pb_{0.4}MnO_3$, annealed in oxygen,[15] exhibit a T_{MI} of 315 K with a T_C above 300 K whereas values of 355 and *ca.* 325 K respectively have been obtained on single crystals of the same nominal stoichiometry.[31] Measurements on polycrystalline materials[28] of nominal compositions $La_{0.9}Pb_{0.1}MnO_3$ and

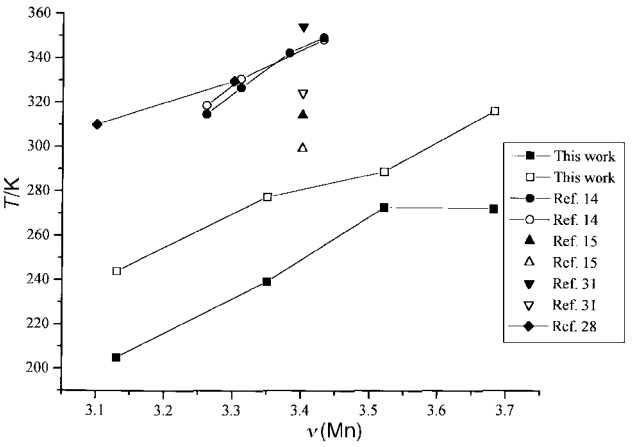

Fig. 7 Variation of T_{MI} (solid points) and T_C (open points) with the mean manganese oxidation state, v(Mn), for samples prepared in this work and for those previously reported. The lines are a guide to the eye and connect T_C/T_{MI} data from the same study.

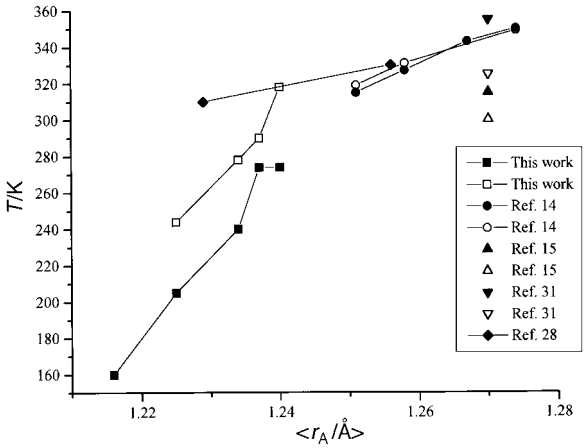

Fig. 8 Variation of T_{MI} (solid points) and T_C (open points) with the average radius of the A-site cations, $\langle r_A \rangle$, for samples prepared in this work and for those previously reported. The lines are a guide to the eye and connect T_C/T_{MI} data from the same study.

$La_{0.7}Pb_{0.3}MnO_3$ place the MI transition at 310 and 330 K, respectively. These reports would appear to suggest that in the composition range corresponding to $0.1 \leqslant x \leqslant 0.4$, T_{MI} and T_C span a fairly narrow range of temperatures. For comparison purposes, these data are included in Fig. 7. For a given oxidation state, T_C/T_{MI} determined here are consistently lower than previous reports would indicate. Furthermore, results presented here span a wider range of temperatures than in previous work, although this range is more comparable with that for the analogous alkaline-earth doped phases for which T_{MI} ranges from 200–270 K (Ca dopant)[32] or 215–325 K (Sr dopant)[13] for similar doping levels. It should be emphasised that values of v(Mn) used in Fig. 7, for samples investigated in previous studies, have been derived from the nominal compositions. These, as we have shown in the present work, may not always be a reliable guide. In addition, some of the data plotted in Fig. 7 correspond to samples in forms other than polycrystalline powders. Inconsistencies between data collected on single crystals, thin films and polycrystalline powders are frequently observed. Indeed, as is evident from Fig. 7, T_{MI} for $La_{0.6}Pb_{0.4}MnO_3$ in single-crystal and thin-film material differs by 40 K. Particle-size effects have also been shown to contribute to variations observed in T_{MI} determined for polycrystalline powders.[33,34] However, the more probable explanation for the discrepancies in Fig. 7 is that samples with the same v(Mn) have different La : Pb ratios and hence different microstructural properties. Changes in the Mn—O—Mn bond angles, even

with a constant carrier concentration, will affect T_C. An indication of the structural influence may be obtained from a plot of T_C/T_{MI} as a function of the weighted A-site cation radius $\langle r_A \rangle$. In Fig. 8, values of T_C/T_{MI} from this and previous studies are plotted as a function of $\langle r_A \rangle$ calculated from tabulated ionic radii.[35] Data from the present study appear to continue the trend of decreasing T_C/T_{MI} with smaller cation radii. A similar trend has been observed in previous investigations of doped manganates[36] and may be attributed to a decrease in the Mn—O—Mn bond angle.

In conclusion, we have shown that contrary to earlier reports, compositional variations of critical temperatures in the lead-doped lanthanum manganates are comparable with those in the corresponding alkaline-earth-doped materials. Significant deviations from nominal stoichiometries are observed, which demonstrates the need to make measurements on chemically well characterised samples, if a consistent theoretical picture is to be realised.

Financial support from the EPSRC and The Royal Society is gratefully acknowledged. We wish to thank Dr A. M. Chippindale, University of Oxford for assistance with the energy dispersive X-ray microanalysis measurements.

References

1 C. N. R. Rao, A. K. Cheetham and R. Mahesh, *Chem. Mater*., 1996, **8**, 2421.
2 S. Jin, T. H. Tiefel, M. McCormack, R. A. Fastnacht, R. Ramesh and L. H. Chen, *Science*, 1994, **264**, 413.
3 S. Jin, M. McCormack, T. H. Tiefel and R. Ramesh, *J. Appl. Phys*., 1994, **76**, 6929.
4 B. Raveau, A. Maignan and V. Caignaert, *J. Solid State Chem*., 1995, **117**, 424.
5 R. M. Kusters, J. Singleton, D. A. Keen, R. McGreevy and W. Hayes, *Physica B*, 1989, **155**, 362.
6 R. von Helmolt, J. Wecker, K. Samwer, L. Haupt and K. Bärner, *J. Appl. Phys*., 1994, **76**, 6925.
7 A. J. Millis, P. B. Littlewood and B. I. Shraiman, *Phys. Rev. Lett*., 1995, **74**, 5144.
8 P. Schiffer, A. P. Ramirez, W. Bao and S. W. Cheong, *Phys Rev. Lett*., 1995, **75**, 3336.
9 A. Urushibara, Y. Moritomo, T. Arima, A. Asamitsu, G. Kido and Y. Tokura, *Phys. Rev. B*, 1995, **51**, 14 103.
10 R. L. White, *IEEE Trans. Magn*., 1992, **28**, 2482.
11 K. Chahara, T. Ohno, M. Kasai and Y. Kozono, *Appl. Phys. Lett*., 1993, **63**, 1990.
12 R. von Helmolt, J. Wecker, B. Holzapfel, L. Schultz and K. Samwer, *Phys. Rev. Lett*., 1993, **71**, 2331.
13 R. Mahesh, R. Mahendiran, A. K. Raychaudhuri and C. N. R. Rao, *J. Solid State Chem*., 1995, **114**, 297.
14 C. W. Searle and S. T. Wang, *Can. J. Phys*., 1970, **48**, 2023.
15 S. S. Manoharan, N. Y. Vasanthacharya, M. S. Hegde, K. M. Satyalakshmi, V. Prasad and S. V. Subramanyam, *Appl. Phys*., 1994, **76**, 3923.
16 B. C. Tofield and W. R. Scott, *J. Solid State Chem*., 1974, **10**, 183.
17 J. A. M. van Roosmalen, E. H. P. Cordfunke, R. B. Helmholdt and H. W. Zandbergen, *J. Solid State Chem*., 1994, **110**, 100.
18 B. C. Hauback, H. Fjellvåg and N. Sakai, *J. Solid State Chem*., 1996, **124**, 43.
19 E. O. Wollan and W. C. Koehler, *Phys. Rev*., 1955, **100**, 545.
20 A. Wold and R. J. Arnott, *J. Phys. Chem. Solids*, 1959, **9**, 176.
21 J. Töpfer and J. B. Goodenough, *Chem. Mater*., 1997, **9**, 1467.
22 J. A. M. van Roosmalen, P. van Vlaanderen, E. H. P. Cordfunke, W. L. IJdo and D. J. W. IJdo, *J. Solid State Chem*., 1995, **114**, 516.
23 J. B. Goodenough and J. M. Longo, *Landolt-Bornstein Tabellen, New Ser*., 1970, **3**, 126.
24 J. Töpfer, J. P. Doumerc and J. C. Grenier, *J. Mater. Chem*., 1996, **6**, 1511.
25 J. Töpfer and J. B. Goodenough, *J. Solid State Chem*., 1997, **130**, 117.
26 G. H. Jonker, *J. Appl. Phys*., 1966, **37**, 1424.
27 J. B. Goodenough, *Phys. Rev*., 1955, **100**, 564.
28 R. Mahendiran, R. Mahesh, A. K. Raychaudhuri and C. N. R. Rao, *J. Phys. D*, 1995, **28**, 1743.
29 C. Zener, *Phys. Rev*., 1951, **82**, 403.
30 R. Mahendiran, R. Mahesh, A. K. Raychaudhuri and C. N. R. Rao, *Solid State Commun*., 1996, **99**, 149.
31 Y. X. Jia, L. Lu, K. Khazeni, V. H. Crespi, A. Zettl and M. L. Cohen, *Phys. Rev. B*, 1995, **52**, 9147.
32 J. J. Neumeier, M. F. Hundley, J. D. Thompson and R. H. Heffner, *Phys. Rev. B*, 1995, **52**, R7006.
33 R. Mahesh, R. Mahendiran, A. K. Raychaudhuri and C. N. R. Rao, *Appl. Phys. Lett*., 1996, **68**, 2291.
34 M. Verelst, N. Rangavittal, C. N. R. Rao and A. Rousset, *J. Solid State Chem*., 1993, **104**, 74.
35 R. D. Shannon, *Acta. Crystallogr., Sect. A*, 1976, **32**, 751.
36 R. Mahesh, R. Mahendiran, A. K. Raychaudhuri and C. N. R. Rao, *J. Solid State Chem*., 1995, **120**, 204.

Paper 7/05137I; *Received* 17*th July*, 1997